

Supervised classification using neural networks based on polarimetric time-frequency signatures

M. Duquenoy, J.P. Ovarlez, C. Morisseau, G. Vieillard

ONERA

DEMR department Signal Processing unit

Chemin de la Hunière

F-91761 Palaiseau cedex

Palaiseau, France

Email: ovarlez@onera.fr

L. Ferro-Famil, E. Pottier

IETR

Image and Remote Sensing Group

SAPHIR Team

University of Rennes 1

Rennes, France

Email: laurent.ferro-famil@univ-rennes1.fr

Abstract—This paper suggests a supervised classification process based on polarimetric time-frequency signatures by neural networks. Polarimetric time-frequency signature is obtained by multi-dimensional continuous wavelet transform and polarimetric coherent decomposition. This signature is sent to the neural networks which classifies scatterers in canonical target. The learning basis of the neural network is a set of canonical targets and the classification process is applied on anechoic chamber data. The results show different advantages but it is limited by the learning basis, the angular excursion and the frequency bandwidth.

Conventional radar imaging techniques consider targets as a set of bright points. Indeed, it considers scatterers as isotropic for all the directions of presentation and white in the frequency band[1]. Recent studies showed, using time-frequency analysis, the angular and frequency behavior of the spatial distribution of all image scatterers [2], [3]. These representations, called hyperimages, showed that some scatterers were neither isotropic nor white. For example, this is the case with modern high-resolution SAR sensors using wide bandwidth and wide azimuth beam width. This non-stationary behavior of scatterers can be explained by their material (dispersive), their geometry (anisotropic and dispersive) or their orientation (anisotropic). These studies show that some scatterers are non-stationary in the energetic way.

Polarimetry is another information source about the geometry and the orientation of scatterers in radar imaging. Recent studies showed, using time-frequency analysis and polarimetric coherent decompositions, the polarimetric angular and frequency behavior of the spatial distribution of all image scatterers [4], [5]. These representations, called polarimetric hyperimages, showed that some scatterers were not polarimetric stationary.

The aim of this paper is to classify scatterers according to their energetic or polarimetric behaviors. This paper presents the construction of polarimetric time-frequency signatures. Then, the signature of canonical targets is extracted and a process of classification is designed by neural networks to discriminate data from anechoic chamber.

I. CLASSICAL RADAR IMAGING

The backscattering coefficient $H(\mathbf{k})$ for a given object illuminated by a radar is characterized, for a distance R going to infinity, as the ratio between the incoming field E_r and the emitted field E_i (spherical waves):

$$|H(\mathbf{k})| = \lim_{R \rightarrow \infty} \sqrt{4\pi R^2} \frac{E_r}{E_i}. \quad (1)$$

The squared modulus of $H(\mathbf{k})$ is called the Radar Cross Section (RCS) of the object for the wave vector \mathbf{k} and is expressed in squared meter. Wave vector \mathbf{k} is related to the frequency f and to the direction θ of illumination by $|\mathbf{k}| = k = 2f/c$ and $\theta = \arg(\mathbf{k})$ in two-dimensional approximation.

The model usually used in radar imaging is the model of bright points [6]. The object under analysis can be seen as a set of bright points, i.e. a set of independent sources which reflect in the same way for all frequencies (white points) and all directions of presentation (isotropic points). Let $I(\mathbf{r})$ be the amplitude of the bright point response located at $\mathbf{r} = (x, y)^T$ in a set of cartesian axes related to the object. Under far field conditions (decomposition into plane waves), the complex backscattering coefficient for the whole object is then given by the in-phase summation of each reflector contribution:

$$H(\mathbf{k}) = \int I(\mathbf{r}) e^{-2i\pi\mathbf{k}\cdot\mathbf{r}} d\mathbf{r}. \quad (2)$$

After a Fourier Transform of (2), one can obtain the spatial repartition $I(\mathbf{r})$ of the reflectors for a mean frequency (the center frequency) and for a mean angle of presentation:

$$I(\mathbf{r}) = \int H(\mathbf{k}) e^{2i\pi\mathbf{k}\cdot\mathbf{r}} d\mathbf{k}. \quad (3)$$

When a target is illuminated by a broad-band signal and/or for a large angular extent, it is realistic to consider that the amplitude spatial repartition $I(\mathbf{r})$ of the reflectors depends on frequency f and on aspect angle θ . This repartition depending on the wave vector \mathbf{k} , it will be noted in the following by $\tilde{I}(\mathbf{r}, \mathbf{k})$.

II. EXTENDED RADAR IMAGING

A. Construction of the hyperImage based on the continuous wavelet

Let $\phi(\mathbf{k})$ be a mother wavelet supposed to represent the signal reflected by a reference target. This target is supposed located around $\mathbf{r} = \vec{0}$ and backscatters the energy in the direction $\theta = 0$ and at the frequency f given by $k = \frac{2f}{c} = 1$. A family of function is built $\Psi_{\mathbf{r}_o, \mathbf{k}_o}$ from $\phi(\mathbf{k})$ by the similarity group S [2], [3] :

$$\begin{aligned} \Psi_{\mathbf{r}_o, \mathbf{k}_o}(\mathbf{k}) &= \frac{1}{k_o} e^{-j2\pi\mathbf{k}\cdot\mathbf{r}_o} \phi\left(\frac{1}{k_o}\mathcal{R}_{\theta_o}^{-1}\vec{k}\right) \\ &= \frac{1}{k_o} e^{-j2\pi\mathbf{k}\cdot\mathbf{r}_o} \phi\left(\frac{k}{k_o}, \theta - \theta_o\right). \end{aligned} \quad (4)$$

The wavelet coefficient $C_H(\mathbf{r}_o, \mathbf{k}_o)$ is defined as the scalar product between the complex backscattering coefficient H and the wavelet $\Psi_{\mathbf{r}_o, \mathbf{k}_o}$:

$$C_H(\mathbf{r}_o, \mathbf{k}_o) = \langle H, \Psi_{\mathbf{r}_o, \mathbf{k}_o} \rangle \quad (6)$$

The scalar product is defined following [7]:

$$\begin{aligned} C_H(\mathbf{r}_o, \mathbf{k}_o) &= \int_0^{2\pi} d\theta \int_0^{+\infty} k H(k, \theta) \frac{1}{k_o} \\ &e^{+j2\pi\mathbf{k}\cdot\mathbf{r}_o} \phi^*\left(\frac{k}{k_o}, \theta - \theta_o\right) dk \end{aligned} \quad (7)$$

The scalogram which is the square modulus of the wavelet coefficients defines the hyperImage $\tilde{I}_H(\mathbf{r}, \mathbf{k})$.

B. Properties

The continuous wavelet transform has three interesting properties. The first is the reconstruction.

It is possible to build the complex backscattering coefficient $H(\mathbf{k})$ from the wavelet coefficient $C_H(\mathbf{r}_o, \mathbf{k}_o)$:

$$H(\mathbf{k}) = \frac{1}{K_\phi} \int_S d\mathbf{r}_o \int C_H(\mathbf{r}_o, \mathbf{k}_o) \Psi_{\mathbf{r}_o, \mathbf{k}_o}(\mathbf{k}) d\mathbf{k}_o \quad (8)$$

with K_ϕ defined as the *admissibility coefficient* of the mother wavelet which must, to build $H(\mathbf{k})$ from the wavelet coefficients, check:

$$K_\phi = \int |\phi(\mathbf{k})|^2 \frac{d\mathbf{k}}{k^2} < +\infty \quad (9)$$

The second property is the isometry.

$$\frac{1}{K_\phi} \int_S d\mathbf{r}_o \int |C_H(\mathbf{r}_o, \mathbf{k}_o)|^2 d\mathbf{k}_o = \|H\|^2 \quad (10)$$

The third property is the covariance law. The principle of the extended radar imaging is based on a physical group of transformations, the similarity group S that acts on the physical variables \mathbf{r} and \mathbf{k} through rotations $[\mathbf{R}]_\alpha$, dilations a in length (or time) and translations $\delta\mathbf{r}$ as:

$$\begin{aligned} \mathbf{r} &\longrightarrow \mathbf{r}' = a [\mathbf{R}]_\alpha \mathbf{r} + \delta\mathbf{r} \\ \downarrow &\quad \downarrow \\ \mathbf{k} &\longrightarrow \mathbf{k}' = a^{-1} [\mathbf{R}]_\alpha \mathbf{k}. \end{aligned} \quad (11)$$

The transformation law of the reflected signal $H(\mathbf{k})$ and its extended image $\tilde{I}(\mathbf{r}, \mathbf{k})$ is therefore given by:

$$\begin{aligned} H(\mathbf{k}) &\longrightarrow H'(\mathbf{k}) = a \exp(-2i\pi\mathbf{k} \cdot \delta\mathbf{r}) H(a[\mathbf{R}]_\alpha^{-1} \mathbf{k}) \\ \downarrow &\quad \downarrow \\ \tilde{I}(\mathbf{r}, \mathbf{k}) &\longrightarrow \tilde{I}'(\mathbf{r}, \mathbf{k}) = \tilde{I}(a^{-1} [\mathbf{R}]_\alpha^{-1} (\mathbf{r} - \delta\mathbf{r}), a [\mathbf{R}]_\alpha^{-1} \mathbf{k}). \end{aligned} \quad (12)$$

This covariance law is the invariance of the form of physical laws under arbitrary differentiable coordinate transformations. The essential idea is that coordinates do not exist *a priori* in nature, but are only artifices used in describing nature, and hence should play no role in the formulation of fundamental physical laws.

So, in radar imaging, the change of reference coordinates usually is an origin change (translations $\delta\mathbf{r}$), the orientation of axis change (rotations $[\mathbf{R}]_\alpha$), and a scale change (dilations a in length (or time)). For two different observers \mathcal{A} and \mathcal{B} connected by the transformation law (11) (\mathbf{r} is the coordinates of \mathcal{A} and \mathbf{r}' is the coordinates of \mathcal{B}), the coordinates of the wave vector are achieved according to (11). $H(\mathbf{k})$ is the backscattering coefficient measured by \mathcal{A} and $H'(\mathbf{k})$ is the backscattering coefficient measured by \mathcal{B} , these two coefficients are connected by the law (12). To respect the covariance law, the extended image must follow the relation (12).

III. POLARIMETRIC HYPERIMAGES

A full polarimetric radar is generally designed to transmit and receive microwave radiations horizontally (h) or vertically (v) polarized. The polarimetric generalization of the scattering coefficient is called the scattering matrix $[\mathbf{S}]$ or Sinclair matrix:

$$[\mathbf{S}] = \begin{bmatrix} S_{hh} & S_{hv} \\ S_{vh} & S_{vv} \end{bmatrix}. \quad (13)$$

The wavelet transform (6) is applied on each of the four polarimetric channels. The resulting Sinclair scattering matrix now depends on the frequency and on the illumination angle and is called hyper-scattering matrix:

$$[\mathbf{S}](\mathbf{r}, \mathbf{k}) = \begin{bmatrix} S_{hh}(\mathbf{r}, \mathbf{k}) & S_{hv}(\mathbf{r}, \mathbf{k}) \\ S_{vh}(\mathbf{r}, \mathbf{k}) & S_{vv}(\mathbf{r}, \mathbf{k}) \end{bmatrix}. \quad (14)$$

By applying the polarimetric coherent decompositions to the hyper-scattering matrix, we obtain, on one hand, a polarimetric evolution of the scatterers versus emitted frequency and observation angle, on the other hand a polarimetric spatial response for each frequency and angle of illumination. This defines the polarimetric hyperimage concept [4], [5] see 1.

A. Extended Span

The span is generally defined as the sum of the squared modulus of each element of the matrix (13). The extended span is now defined as the sum of the squared modulus of each element of the hyper-scattering matrix (14).

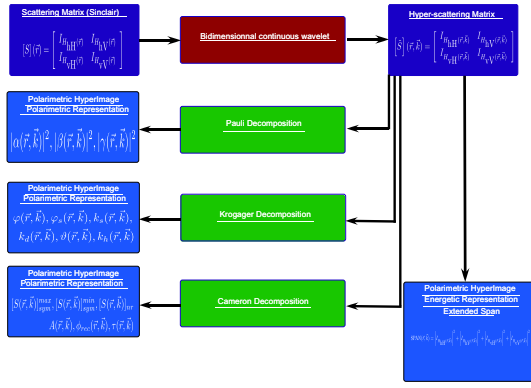


Fig. 1. Algorithm process to obtain polarimetric hyperimages

B. Pauli Hyperimages

By applying the Pauli decomposition [8] to the hyper-scattering matrix, we obtain three interesting coefficients. For each \mathbf{k}_0 , (i.e. for an emitted frequency and for an observation angle), $|\alpha(\mathbf{r}, \mathbf{k}_0)|^2$ (respectively $|\beta(\mathbf{r}, \mathbf{k}_0)|^2$, $|\gamma(\mathbf{r}, \mathbf{k}_0)|^2$) represents the spatial repartition of the targets characterized by single or odd-bounce (respectively double or even-bounce, volume scattering).

For each \mathbf{r}_0 , $|\alpha(\mathbf{r}_0, \mathbf{k})|^2$ (respectively $|\beta(\mathbf{r}_0, \mathbf{k})|^2$, $|\gamma(\mathbf{r}_0, \mathbf{k})|^2$) represents the single or odd-bounce response (respectively double or even-bounce response, volume scattering response) relative to the illumination angle and to the emitted frequency of the scatterer located at \mathbf{r}_0 .

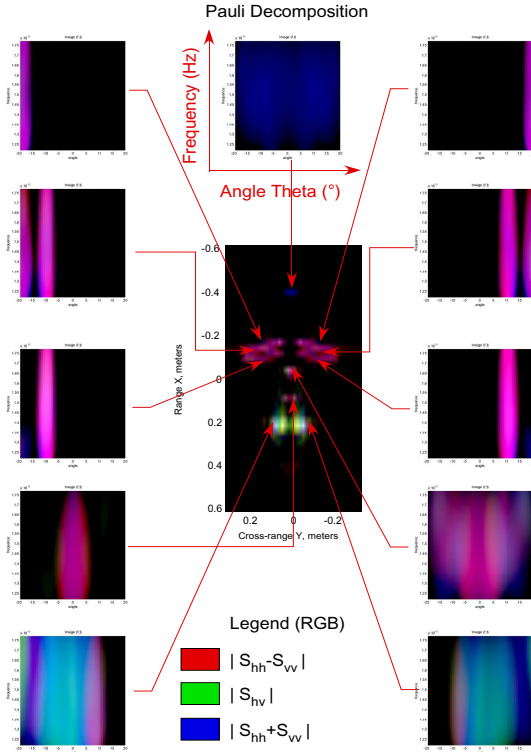


Fig. 2. Time-frequency polarimetric signatures extracted from the Pauli Hyperimage

C. Krogager Hyperimages

By evaluating the hyper-scattering matrix with the Krogager decomposition [9],[10], we obtain three interesting coefficient. For each \mathbf{k}_0 , the coefficients $|k_s(\mathbf{r}, \mathbf{k}_0)|^2$, $|k_d(\mathbf{r}, \mathbf{k}_0)|^2$, $|k_h(\mathbf{r}, \mathbf{k}_0)|^2$ are interpreted as the power scattered by the sphere, the diplane and the helix components, for an emitted frequency and for an observation angle. The phase parameter $\vartheta(\mathbf{r}, \mathbf{k}_0)$ stands for the orientation angle of the diplane and helix components. The phases $\varphi(\mathbf{r}, \mathbf{k}_0)$ and $\varphi_s(\mathbf{r}, \mathbf{k}_0)$ have no signification.

For a given \mathbf{r}_0 , the parameters $|k_s(\mathbf{r}_0, \mathbf{k})|^2$, $|k_d(\mathbf{r}_0, \mathbf{k})|^2$, $|k_h(\mathbf{r}_0, \mathbf{k})|^2$ express the sphere, diplane, helix responses versus emitted frequency and observation angle of the scatterer located at \mathbf{r}_0 . The phase parameter $\vartheta(\mathbf{r}_0, \mathbf{k})$ is interpreted as the evolution of the orientation angle of the diplane and helix components.

D. Cameron Hyperimages

By analyzing the hyper-scattering matrix with the Cameron decomposition [11], [12], we obtain a new classification hyperimage $W(\mathbf{r}, \mathbf{k})$ and allows to extract the Huynen orientation $\psi(\mathbf{r}, \mathbf{k})$.

For each \mathbf{k}_0 , the classification hyperimage and the Huynen orientation represent the classification and the orientation of the target around the line of sight for an illumination angle and for an emitted frequency.

For each \mathbf{r}_0 , the classification hyperimage and the Huynen orientation express the polarimetric behavior evolution and the angle in the vertical plane of the scatterer located at \mathbf{r}_0 .

IV. CLASSIFICATION PROCESS

All in all, for each reflector located at $\mathbf{r}_0 = (x_0, y_0)^T$, we can extract its feature $\tilde{I}(x_0, y_0, f, \theta)$ for each frequency f and for each angle θ . This aspect is the one we have decided to point out in order to see if this quantity can be interpretable in terms of target characteristics. This signature is called polarimetric time-frequency signature.

A. The multi-layer Perceptron

A multi-layer perceptron is a feedforward artificial neural network model that maps sets of input data onto a set of appropriate output. The structure of our multi-layer perceptron is described figure (3). It is composed of nodes whose the processing is :

$$a_j^{(1)} = \sum_{i=1}^d w_{ij}^{(1)} x_i + b_j^{(1)} \quad (15)$$

Where $a_j^{(1)}$ associated input with each hidden unit. Here $w_{ij}^{(1)}$ represents the elements of the first-layer weight matrix and b_j are the bias parameters associated with the hidden unit. The variables $a_j^{(1)}$ are then transformed by the non-linear activation function of the hidden layer. The activation function is tanh. The outputs of the hidden units are given by :

$$z_j = \tanh(a_j^{(1)}) \quad (16)$$

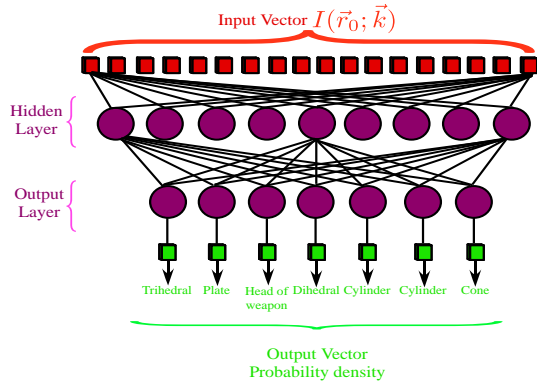


Fig. 3. Architecture of the multi-layer perceptron

which has the property that :

$$\frac{dz_j}{da_j^{(1)}} = 1 - z_j^2 \quad (17)$$

The z_j are then transformed by the second layer of weights and biases to give second-layer activation values $a_k^{(2)}$:

$$a_k^{(2)} = \sum_{j=1}^M w_{ij}^{(2)} z_j + b_k^{(2)} \quad (18)$$

Finally, these values are passed through the output-unit activation function to give output values y_k . For the more usual kind of classification problem in which we have of c mutually exclusive classes, we use the softmax activation function of the form :

$$y_k = \frac{\exp(a_k^{(2)})}{\sum_{k'} a_k^{(2)}} \quad (19)$$

Our multi-layer perceptron is a three layers whose the number of nodes of the input layer is equal to the number of input, the output layer is equal to the number of class to obtain a probability density whose the maximum defines the class which the scatterer is and the number of nodes of the hidden-layer is calculated following :

$$N_{Hidden-Layer} = \sqrt{N_{input} N_{output}} \quad (20)$$

B. The learning Basis

The learning basis is composed of seven canonical targets : trihedral, dihedral, head of weapon, plate, two cylinders, and cone. The backscattering coefficient is measured for a frequency bandwidth between 12 GHz and 18 GHz with a sampling step of 7.50 MHz and for an angular excursion between -20 and 20 with a sampling step of 0.5 . From the image the polarimetric time-frequency signatures are extracted and selected manually. Then, the signature is translated in the angle domain to release the orientation phenomena. Indeed, two scatterers of same nature with different orientation must have the same classification. This learning basis is sent to the neural network for a supervised learning based on the scaled conjugate gradient algorithm.

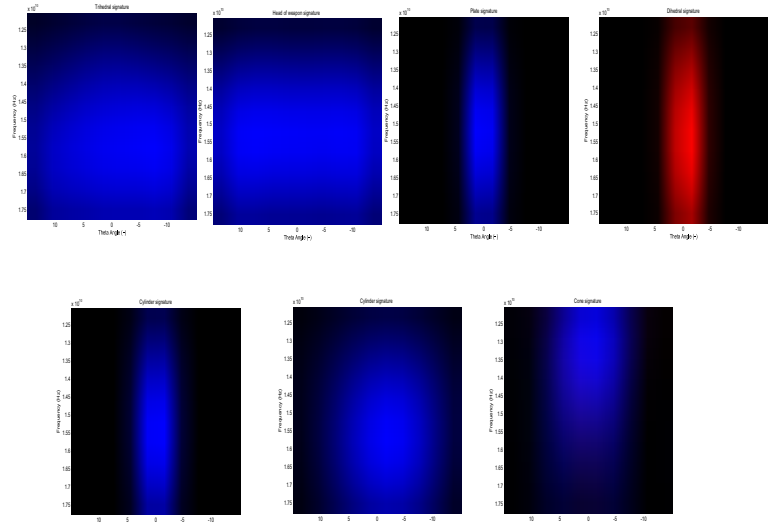


Fig. 4. Learning basis of time-frequency polarimetric signatures extracted from the Pauli Hyperimage

V. RESULTS

The target under study is a "Cyrano" weapon model in steel. The backscattering coefficient is measured for a frequency bandwidth between 12 GHz and 18 GHz with a sampling step of 7.50 MHz and for an angular excursion between -20 and 20 with a sampling step of 0.5 . From the image the polarimetric time-frequency signatures are extracted and sent to the neural network.

A. Extended Span results

The results of the extended span are represented on the figure (5). The head of "Cyrano" is classified as a head of weapon. The trailing edges of wing are identified as dihedral. It can be explained by the fact the responses of the edges and of diplane are directive responses. The closed air exit is classified as a specular plate because the response is directive. The open air intake is identified as a head of weapon because the polarimetric time-frequency signature is isotropic and non-dispersive. For the stabilizers the classification is a melting pot of cylinder, head of weapon and cone contribution.

B. Pauli time-frequency signatures results

The results of the Pauli hyperimage are represented on the figure (6). The head of "Cyrano" is classified as a head of weapon. The trailing edges of wing are identified as dihedral or plate. It can be explained by the fact the responses of the edges are directive responses with a melting pot of simple bounce and double bounce contribution. The closed air exit is classified as a specular plate because the response is directive. The open air intake is identified as a cylinder because the polarimetric time-frequency signature is isotropic and non-dispersive. For the stabilizers the classification is a melting pot of cylinder, head of weapon and plate.

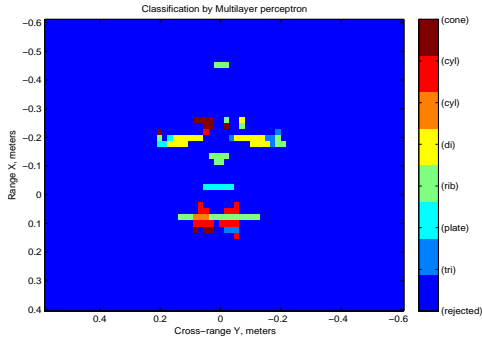


Fig. 5. Classifications results obtained by the multi-layer perceptron in using the extended Span

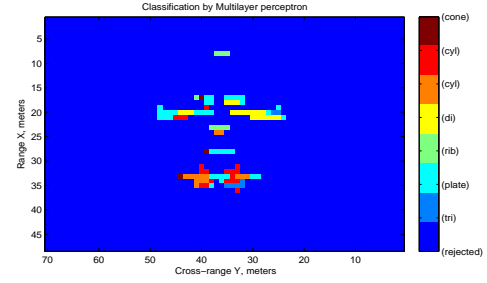


Fig. 7. Classifications results obtained by the multi-layer perceptron in using the Krogager Hyperimage

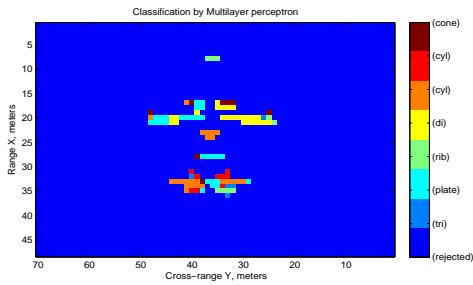


Fig. 6. Classifications results obtained by the multi-layer perceptron in using the Pauli Hyperimage

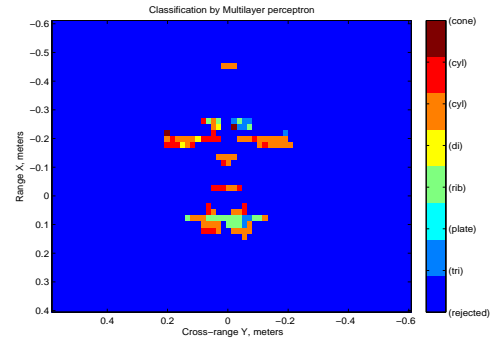


Fig. 8. Classifications results obtained by the multi-layer perceptron in using the Cameron Hyperimage

C. Krogager time-frequency signatures results

The results of the Krogager hyperimage are represented on the figure (7). The head of "Cyrano" is classified as a head of weapon. The trailing edges of wing are identified as dihedral or plate. It can be explained by the fact the responses of the edges are directive responses with a melting pot of simple bounce and double bounce contribution. The closed air exit is classified as a specular plate because the response is directive with a simple bounce behavior. The open air intake is identified as a cylinder because the polarimetric time-frequency signature is isotropic and non-dispersive. For the stabilizers the classification is a melting pot of cylinder, head of weapon and plate.

D. Cameron time-frequency signatures results

The results of the Cameron hyperimage are represented on the figure (8). These results are not convincing. Indeed, the Cameron hyperimage is composed by a set of polarimetric classes and our learning basis is not sufficient.

VI. CONCLUSION

Usually, radar imaging considers scatterers as a set of "bright points". However new applications using a wide bandwidth and a large angular excursion does not make this assumption. Multi-dimensional time-frequency highlights this point of

view. Polarimetry gives some informations on the geometry and on the orientation. The joint using multi-dimensional analysis and polarimetric coherent decomposition allow to extract polarimetric time-frequency signatures.

These polarimetric time-frequency signatures explain the non-stationnary behaviors of scatterers and are an information source. The goal of this paper is to use the polarimetric time-frequency signatures to classify scatterers.

In this paper, a supervised classification is proposed. The learning basis is a set of canonical targets whose the backscattering center is selected manually. So, a neural network is trained by the learning basis. The anechoic chamber data are feedforward to the multi-layer perceptron.

The results show that polarimetric time-frequency signatures allow to characterize scatterers. However, our learning basis is not sufficient to compare these results to the coherent decomposition.

ACKNOWLEDGMENT

The authors would like to thank the unit DEMR-FUR to provide data.

REFERENCES

- [1] M. Soumekh, *Fourier Array Imaging*. Englewood Cliffs: Prentice Hall, 1994.

- [2] J. Bertrand and P. Bertrand, "The concept of hyperimage in wide-band radar imaging," *IEEE Trans. Geosci. Remote Sensing*, vol. 34, no. 5, pp. 1144–1150, Sep. 1996.
- [3] J. P. Ovarlez, L. Vignaud, J. C. Castelli, M. Tria, and M. Benidir, "Analysis of sar images by multidimensional wavelet transform," *IEE Proc. Radar. Sonar. Navig.*, vol. 150, no. 4, pp. 234–241, Aug. 2003.
- [4] M. Duquenoy, J. Ovarlez, L. Ferro-Famil, L. Vignaud, and E. Pottier, "Study of dispersive and anisotropic scatterers behavior in radar imaging using time-frequency analysis and polarimetric coherent decomposition," in *Proc. IEEE radar conference*, Verona, USA, Apr. 24–27, 2006, pp. 180–185.
- [5] —, "Study of dispersive and anisotropic scatterers behavior in radar imaging using time-frequency analysis and polarimetric coherent decompositions," in *Proc. sixth European Conference on Synthetic Aperture Radar (EUSAR'06)*, Dresden, Germany, May 16–18, 2006.
- [6] D. Mensa, *High Resolution Radar Imaging*. USA: Artech House, 1981.
- [7] M. Tria, "Imagerie radar synthèse d'ouverture par analyse en ondelettes continues multidimensionnelles," Ph.D. dissertation, Univ. of Paris-Sud, Paris, France, Nov. 2005.
- [8] V. Alberga, E. Krogager, M. Chandra, and G. Wanielik, "Potential of coherent decompositions in sar polarimetry and interferometry," in *Proc. IEEE International Geoscience and Remote Sensing Symposium (IGARSS'04)*, vol. 3, Anchorage, USA, Sep. 20–24, 2004, pp. 1792–1795.
- [9] E. Krogager and Z. H. Czyz, "Properties of the sphere, diplane, helix decomposition," in *Proc. Third International Workshop on Radar Polarimetry (JIPR'1995)*, vol. 1, Nantes, France, Mar. 21–23, 1995, pp. 106–114.
- [10] E. Krogager, J. Dall, and S. N. Madsen, "The sphere, diplane, helix decomposition recent results with polarimetric sar data," in *Proc. Third International Workshop on Radar Polarimetry (JIPR'1995)*, vol. 2, Nantes, France, Mar. 21–23, 1995, pp. 621–625.
- [11] W. L. Cameron, N. N. Youssef, and L. K. Leung, "Simulated polarimetric signatures of primitive geometrical shapes," *IEEE Trans. Geosci. Remote Sensing*, vol. 34, no. 3, pp. 793–803, May 1996.
- [12] W. L. Cameron and H. Rais, "Conservative polarimetric scatterers and their role in incorrect extensions of the cameron decomposition," *IEEE Trans. Geosci. Remote Sensing*, vol. 44, no. 12, pp. 3506–3516, Dec. 2006.